

Received May 18, 2019; reviewed; accepted September 17, 2019

## An investigation of continuous interaction process between air bubble and various roughness coal surfaces using microbalance

Zhimin Guo <sup>1,2,3</sup>, Jianguo Yang <sup>2,3</sup>, Yuling Wang <sup>2,3</sup>

<sup>1</sup> Key Laboratory of Coal Processing and Efficient Utilization of Ministry of Education, China University of Mining and Technology, Xuzhou, Jiangsu 221116, China

<sup>2</sup> School of Chemical Engineering and Technology, China University of Mining and Technology, Xuzhou, Jiangsu 221116, China

<sup>3</sup> National Engineering Research Center of Coal Preparation and Purification, China University of Mining and Technology, Xuzhou, Jiangsu 221116, China

Corresponding authors: scetyjg@126.com (Jianguo Yang), wylcumt@163.com (Yuling Wang)

**Abstract:** Surface roughness of particles plays an important role in bubble-particle interaction process. However, the continuous attachment and detachment process have rarely been characterized between the surface of different roughness and air bubble. In this study, the continuous attachment and detachment processes between the surface of different roughness and air bubble were investigated by a highly sensitive microbalance. The bubble-surface interaction process was monitored by a high-speed camera to analyze the geometry parameters, including distance, adhesion diameter, and contact angle. It was found that the bubble-particle attachment time increased with the increase of surface roughness. The magnitude of the repulsive force in the bubble-surface approaching process increased with the increase of surface roughness, while the attractive force in the bubble-particle retracting process decreased monotonically with the surface roughness. The force measured by microbalance was finally compared with the calculated one. The calculated force at the biggest force point also increased with the decrease of surface roughness. These results indicate that coal particles with lower surface roughness, which have less water-filled pores and pillars, is more conducive to flotation due to the lower repulsive force in the bubble-particle attachment process and higher adhesive force in the bubble-particle detachment process, and vice versa.

**Keywords:** surface roughness, air bubble, contact angle, continuous interaction

### 1. Introduction

Froth flotation technology, which is widely applied to separate various kinds of minerals from each other based on their surface wettability differences, is widely used in mineral and coal processing (Erbil, 2014; Liu and Peng, 2014). In flotation process, the hydrophobic particles can be easily captured by air bubbles, and transported forward into the foam product, while the hydrophilic particles are difficult to be captured by air bubbles, hence remaining in the pulp as tailings (Pietrzak and Wachowska, 2006; Wang et al., 2017; Xing et al., 2017). The interaction between air bubble and particle in the pulp is the key for successful flotation. It has been proposed that the heterogeneities in chemical composition of particles (Drelich et al., 1996; Gosiewska et al., 2002; Karakashev et al., 2011; David and Neumann, 2013; Chang et al., 2017), physical characteristics such as surface roughness (Krasowska and Malysa, 2007; Adams et al., 2008; Feng and Nguyen, 2017), particle shape (Ulusoy et al., 2003; Xia, 2017a), and particle size (Chipfunhu et al., 2011; Han et al., 2014) would complicate the wetting behavior (Bormashenko, 2019), and affect the individual steps of bubble-particle interaction (Chau et al., 2009; Drelich and Marmur, 2017).

In recent years, a surge of deserved attention has been paid to understand the influence of morphological characteristics of particles, especially surface roughness (Osasere Orumwense, 1998; Guven et al., 2015; Xia, 2017b; Drelich, 2018), on the bubble-particle interaction process. Guven et al. (2015) studied the flotation of spherical methylated roughened glass particles. They demonstrated that the rougher the particles, the higher the flotation rate constant. Meanwhile, they proposed for the first time that the size of nanoscale hydrophobic asperities distributed over spherical microscopic particles indicated the magnitude of the energetic barrier that particles needed to overcome in order to attach on bubbles. Wang et al. (2018) investigated the expansion velocity of a three-phase contact line (TPCL) and the terminal diameter of bubbles on low-rank lump coal surfaces of different roughness. The results confirmed that wetting film diameter became smaller, and the expansion velocity of the three-phase contact line was faster with the increasing surface roughness. Chen et al. (2018) analysed the induction time and contact angle of different rough coking coal and anthracite. They identified that the induction time increased with the increasing of surface roughness while the contact angle decreased with it. To date, the influence of surface roughness on the continuous bubble-particle attachment and detachment process has rarely been demonstrated.

Great progress has been made in measuring adhesion force between air bubble/water droplet and solid particle/surface as the development of micro-force measurement system in recent years. For example, Samuel et al. (2011) studied the adhesion force between water droplet and 20 kinds of surfaces using a microelectromechanical balance. The results demonstrated that the snap-in force consistently decreased as the advancing contact angle (CA) decreased, and became zero when the advancing CA was larger than 150°, while the pull-off force was shown to decrease consistently as the receding CA increased. Sun et al. (2017, 2018) measured the adhesion force between water droplet and smooth and patterned polymers (isotropy and anisotropy). They proposed a modified for calculation model for isotropic surfaces, which contained normalized contact line length.

In this study, low-ash anthracite coal clumps of different surface roughness were prepared. Then, a high-sensitive microbalance coupled with a high-speed video camera was used to analyze the continuous attachment and detachment process between air bubble and anthracite surface of various roughness. Better understanding of the continuous interaction between air bubble and coal surface of various roughness may potentially offer a new thought for altering the interactions by a particular design of the surface.

## **2. Materials and methods**

### **2.1. Materials**

The anthracite coal sample was collected from the Taixi Coal Preparation Plant, in Ningxia Province, China. Coal lumps with a diameter of around 10 mm and with density fraction of  $< 1.35 \text{ g/cm}^3$  were used to eliminate the heterogeneity effect on the coal surface. The proximate and ultimate analyses of the coal samples are provided in Table 1. As presented in Table 1, the ash content of the anthracite sample was only 2.18%, indicating negligible amount of impurity minerals in the sample.

The anthracite lump was inlaid in polymer at room temperature. Then, the latter was polished by the MP-2B polish-grinding machine (Lanchou, China) with sandpapers until a fresh flat coal surface exposed. Sandpaper with meshes of 100, 360, 2000, and 5000 was used in this experiment. For convenience, the samples with four degrees of surface roughness were designated as R100, R360, R2000, and R5000, respectively.

### **2.2. Methods**

#### **2.2.1. Surface morphology and component measurements**

The surface morphology and component of coal sample of different roughness were analyzed by SEM (FEI Quanta TM 250, USA) coupling with Energy Dispersive Spectroscopy (EDS). Each polished coal surface was cleaned with pure ethyl alcohol and air dried before each measurement.

To obtain the functional group on the coal surface of different roughness, a Vertex 80v Fourier Transform Infrared Spectroscopy (FTIR) (Bruker, Germany) was used to analyze the sample surface

with reflection mode. The polished coal surfaces were also cleaned with pure ethyl alcohol and air dried before each measurement.

Table 1. Proximate analysis and ultimate analysis of coal samples

Proximate analysis (%)				Ultimate analysis (%)				
$M_{ad}$	$A_{ad}$	$V_{ad}$	$FC_{ad}$	$S_{t,d}$	$O_{daf}$	$C_{daf}$	$H_{daf}$	$N_{daf}$
0.64	2.18	6.98	90.20	0.17	3.22	92.24	3.47	0.89

### 2.2.2. Surface roughness measurements

Surface roughness was quantified by a Mitutoyo SJ-210 profilometer (Japan). The roughness index  $R_a$  was achieved to show the degree of roughness of different flat surfaces. Each coal surface was measured more than three times, and the average  $R_a$  was reported.

### 2.2.3. Contact angle measurements

The advancing and receding contact angles of coal surfaces of different roughness were measured with a JR2000D goniometer. The static bubble captive technique was used in which the bubble size was controlled by injecting and withdrawing air by a micro-syringe that had an U-shaped needle (Drelich et al., 1996). Together with the optical system of the JR2000D goniometer, a shape analysis software was used to measure the advancing and receding contact angles. The measurement system was equipped with a rotatable independent state to guarantee that the surface under measurement was horizontal. For consistency, the contact angle in the direction that was perpendicular to the grooves on coal surface of different roughness was measured, as shown in Fig. 1 (a). The average of more than five independent measurements was reported in this study. The schematic of the measurement process is illustrated in Fig. 1 (b).

### 2.2.4. Continuous interactions process measurements

The continuous attachment and detachment interaction between air bubble and coal surface of different roughness were measured by a high-sensitivity microbalance (XS105 with 0.01 mg accuracy, Mettler Toledo, USA). A 10  $\mu$ L air bubble was formed with a micro-scale syringe above a flat Teflon plate in a beaker filled with ultrapure water with resistivity of 18.2 M  $\Omega$ ·cm<sup>-1</sup> (Canrex Analytic Instrument Ltd., China). The beaker was put on the elevating table, which was controlled to move upward or downward with a velocity range from 0 to 195.56 mm/s by a computer. The coal sample was attached to the measurement hook. The net force of this balance was initialized to zero before every measurement. Obviously, the result measured by microbalance is about mass, hence, the force can be calculated in the way of mass multiply by gravity acceleration,  $g$  (9.8 N/kg). Furthermore, the influence of buoyancy and gravity was eliminated by subtracting background test results, and the background test was conducted without air bubble formed above the flat Teflon plate.

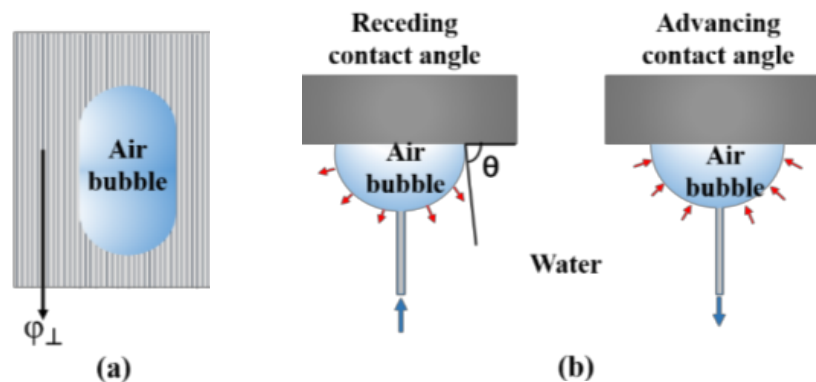


Fig. 1. Analysis direction of contact angle: perpendicular ( $\varphi_{\perp}$ ) with the grooves (a) Schematic of measuring the advancing and receding contact angle (b)

During force measurement, the elevating table first moved upward to make the bubble attract on the coal surface, then the elevating table was maintained for 8 sec before it moved downward for a distance of 8 mm to retract the bubble from the coal surface. The elevating table was moved upward and downward under a given velocity of 0.487 mm/s. When the elevating table was moved upward for a distance of 0.974 mm, the coal surface was compressed the air bubble on the flat Teflon plate. A high-speed video camera was applied to record the attachment and detachment processes. A schematic of the measurement system is shown in Fig. 2. The adhesion diameter, radius of air bubbles, surface curvature, and contact angles of the bubble in the interaction process were analyzed by Image J software. Meanwhile, the distance between coal surface and air bubble at different points was also measured.

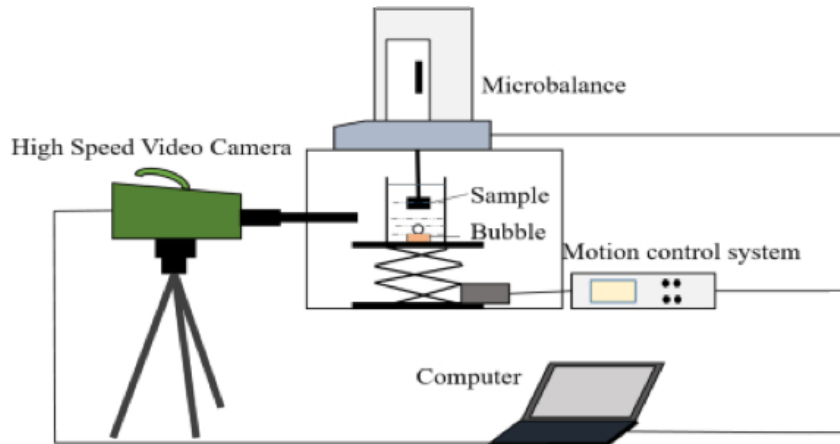


Fig. 2. Schematic of the bubble-particle continuous interaction measurement system

### 3. Results and discussion

#### 3.1. Analysis of surface morphology and components

The surface morphologies of the coal samples of different surface roughness are shown in Fig. 3. It was observed that many ridges and grooves occurred on the polished surfaces which were polished by the polish-grinding machine presented unidirectional. The width and depth of ridges and grooves on the surfaces decreased with the increase of sandpaper meshes. In other words, the sample surface that polished by sandpaper of 5000 mesh was the smoothest, and the surface polished by sandpaper of 100 mesh was the roughest.

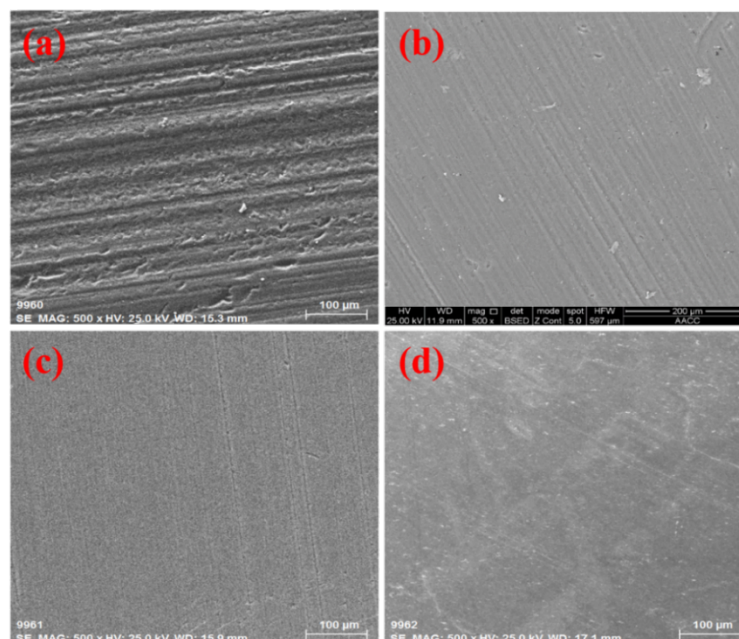


Fig. 3. Surface morphologies of coal surface of different roughness (a) R100 (b) R360 (c) R2000 (d) R5000

The element composition of the samples was measured by SEM coupled with EDS. As seen from Fig. 4. that the coal surfaces of different roughness mainly contained three types of elements, i. e., C, N, and O. None of the Ca, Mg or Al could be detected in the samples. Therefore, the heterogeneity of hydrophilic mineral particles on these coal surfaces during the force measurements can be neglected.

Figure 5 presents the FTIR spectra of coal surfaces of different roughness. Peaks near  $3742\text{ cm}^{-1}$  and  $3642\text{ cm}^{-1}$  are ascribed to absorption of hydrogen bond between O-H groups of alcoholic or phenolic hydroxyl groups in coal molecules (Xia et al., 2014). Peaks around  $2803\text{--}2996\text{ cm}^{-1}$  are corresponding to the broad infrared absorption band of aliphatic  $\text{CH}_x$  (Liu et al., 2017), and the peak near  $1642\text{ cm}^{-1}$  is due to  $\text{C}=\text{O}$  stretching vibration of carbonyl group in carboxylic acid (Chen et al., 2017; Zhou et al., 2019). The peak around  $1600\text{ cm}^{-1}$  is caused by  $\text{C}\equiv\text{C}$  stretching vibrations in aromatic ring (Chen et al., 2017) and peak at  $906\text{ cm}^{-1}$  is related to  $\text{C-O-R}$  stretching vibration (Liu et al., 2017). The FTIR results suggest that these coal surfaces of different roughness had the same kind of functional groups, and the peak intensity at different wavenumbers was similar. Thus, it can be regarded that these four surfaces of different roughness had the same chemical composition.

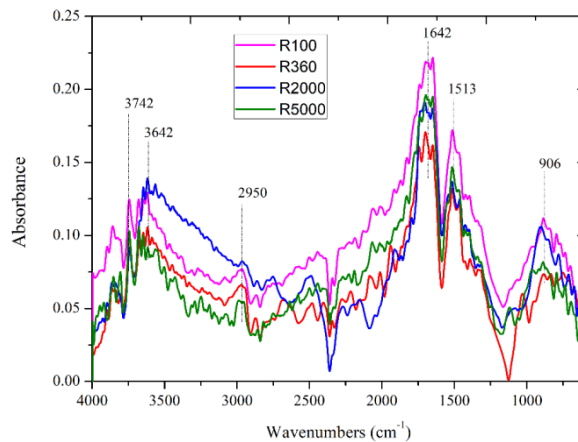


Fig. 4. EDS analysis of coal surfaces of different roughness: (a) R100 (b) R360 (c) R2000 (d) R5000

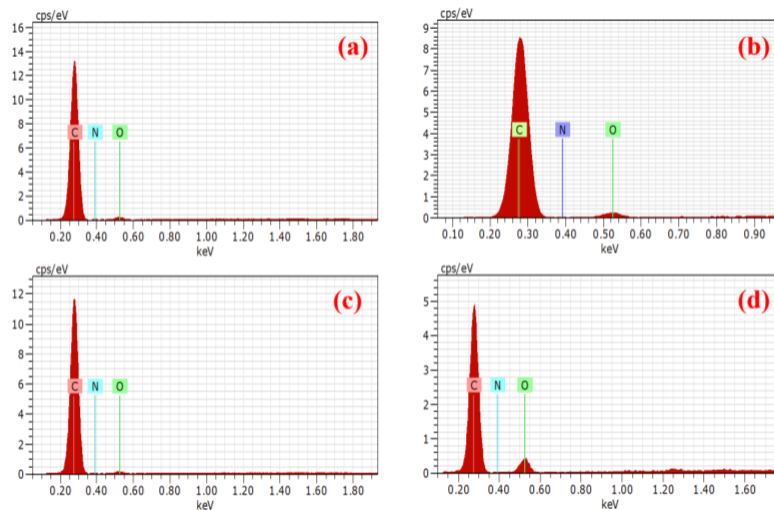


Fig. 5. FTIR spectra of coal surfaces different roughness

### 3.2. Analysis of surface roughness

Coal roughness index on different low-ash surfaces were achieved with the method of a probe of Mitutoyo SJ-210 profilometer moved across the surface. The relationship between index  $R_a$  and sandpaper meshes is shown in Fig. 6. As seen in Fig. 6 that the average roughness index ( $R_a$ ) of R100, R360, R2000, and R5000 surfaces were  $2.51\text{ }\mu\text{m}$ ,  $0.77\text{ }\mu\text{m}$ ,  $0.31\text{ }\mu\text{m}$ , and  $0.12\text{ }\mu\text{m}$ , respectively. The results confirmed that the coal surface polished by the coarser sandpaper possessed higher roughness index.

### 3.3. Analysis of advancing and receding contact angle

Figure 7 presents the results of advancing and receding contact angles of coal surfaces of different roughness. It was detected that both the advancing and receding contact angles decreased with the increase of  $R_a$ . The advancing contact angle steadily decreased from  $93^\circ$  to  $78^\circ$  as the roughness index  $R_a$  increased from  $0.12\ \mu\text{m}$  to  $2.51\ \mu\text{m}$ . Xia (2017b) considered that the proper size of ridges and grooves may prevent the spreading of air bubble, resulting in higher entrapment of water. The ridges and grooves may also present bigger barriers to the motion of three-phase contact line as the degree of roughness increased (Nikolaev, 2016). The receding contact angles of coal surfaces with roughness index of  $2.51\ \mu\text{m}$ ,  $0.77\ \mu\text{m}$ ,  $0.31\ \mu\text{m}$ , and  $0.12\ \mu\text{m}$  were obtained as  $30^\circ$ ,  $47^\circ$ ,  $57^\circ$ , and  $68^\circ$ , respectively. Additionally, the hysteresis contact angle increased from  $26^\circ$  to  $48^\circ$  with the increase of  $R_a$  from  $0.12\ \mu\text{m}$  to  $2.51\ \mu\text{m}$ . Adams et al. (2008) and Johnson et al. (2006) considered that the hysteresis was generally ascribed to roughness and heterogeneity of the surface chemistry. As the samples used in this study were homogeneous in mineral and chemical composition, it can be inferred that the increasing of hysteresis contact angle resulted from the increasing of asperities. The larger hysteresis contact angle was the result of more pinning of the contact line caused by ridges and grooves that make the motion of three-phase contact line exhibit periodic stick-slip behavior (Chung et al., 2007).

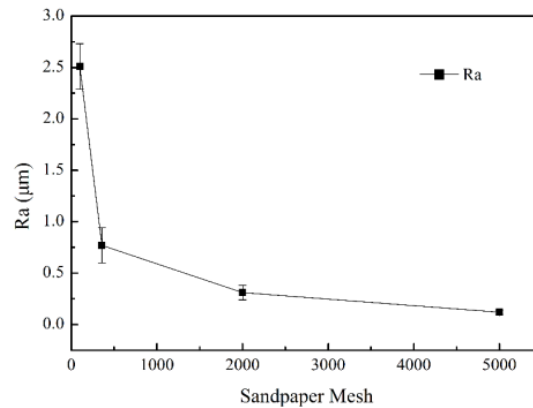


Fig. 6. Relationship between index  $R_a$  and sandpaper mesh

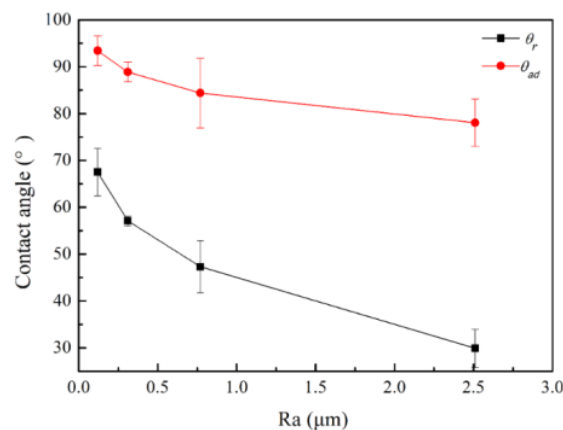


Fig. 7. Advancing and receding contact angles in perpendicular direction on different degrees of roughness

### 3.4. Analysis of the continuous interaction process between coal surface and air bubble

#### 3.4.1. Analysis of interactions in the process of air bubble moving upward

Figure 8 illustrates the force-time profiles between air bubble and the four coal surfaces of different roughness. The bubble contacted primarily with the surface in 0.5 sec. For convenience, the primarily contact point between air bubble and the coal surface and was designated as point A. The interaction forces with the direction of upward increased rapidly in the process of air bubble moving upward, which caused by the deformation of air bubble. There were obvious turning points (designated as point

B) in the four force profiles. The force in the direction of upward reduced slightly after point B. As also shown in Fig. 9 (the force-distance curves), the force magnitude was negative correlated with the distance between air bubble and surface before point B. It suggests that the liquid film has not ruptured before point B. After point B, the rapid expansion of three-phase contact line occurred and caused the reduction of interaction force. Meanwhile, the quick slide of the three-phase contact line was also detected by the high-speed video camera. The attachment time increased with the increasing surface roughness. The turning point of coal surface of R5000 with surface roughness of  $0.12\ \mu\text{m}$  occurred at 0.8 s (Fig. 8) corresponding to the distance of 2.21 mm (Fig. 9), while the turning point occurred at 1.9 sec with surface roughness index of  $2.51\ \mu\text{m}$  (Fig. 8), and the distance between air bubble and sample surface was around 1.68 mm (Fig. 9). Additionally, the occurrence of turning point were 1.3 sec and 1.4 sec, respectively, for the surfaces with rough index  $R_a$  of  $0.31\ \mu\text{m}$  and  $0.77\ \mu\text{m}$ . And, the distance of appearance of turning point between air bubble and rough surface were around 1.92 mm and 1.97 mm, respectively (Fig. 9). The variation trend of the induction time with surface roughness was consistent with that in Chen et al. (2018).

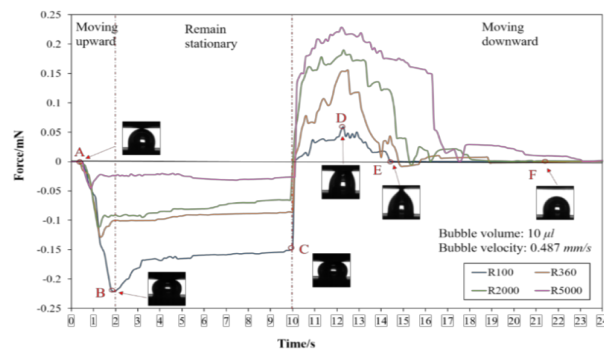


Fig. 8. Force-time profiles between air bubble and the coal surfaces of different degrees of roughness

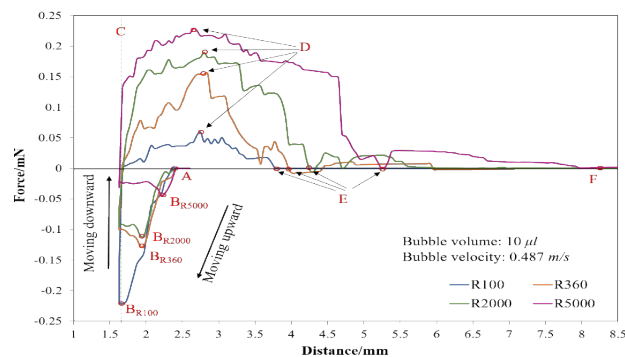


Fig. 9. Force-distance profiles between air bubble and the coal surfaces of different degrees of roughness

Table 2 presents the average values and standard deviation for force magnitude ( $f$ ), adhesion diameter ( $2r_{tpc}$ ), coal surface-evaluating table distance ( $h$ ), and contact angle ( $\theta$ ) during the continuous interaction process between air bubble and coal surface. Note that statistics were measured in the direction that was perpendicular to the grooves.

### 3.4.2. Analysis of interactions in the process of air bubble remained stationary

After moving upward for a distance of 0.974 mm, the elevating table was stopped and remained stationary for 8 sec. The last point of stationary period was referenced as point C. The interaction state between air bubble and the coal surfaces at point C is shown in Fig. 10 which shows that the greatest deformation of air bubble occurred on R100. And, the adhesion diameter ( $2r$ ) decreased with the increasing of surface roughness. As presented in Table 2, the adhesion diameter between air bubble and coal surfaces of R100, R360, R2000, and R5000 were 1.06 mm, 1.44 mm, 1.73 mm, and 1.78 mm, respectively.

Table 2. The average values and standard deviation for force magnitude ( $f$ ), adhesion diameters ( $2r_{tpc}$ ), coal surface-evaluating table distance ( $h$ ), and contact angles ( $\theta$ ) measured during the continuous interactions process

Surfaces		Point C	Biggest force point D	Pull-off point E	Surfaces		Point C	Biggest force point D	Pull-off point E
R100	$h$ (mm)	1.63	2.84	3.72	R2000	$h$ (mm)	1.63	2.75	4.13
	$2r_{tpc}$ (mm)	1.06	0.68	0.24		$2r_{tpc}$ (mm)	1.73	1.12	0.36
	$\theta$ (°)	31.00	63.00	68.00		$\theta$ (°)	64.00	91.00	108.00
	$f$ ( $\mu$ N)	150 $\pm$ 10	53 $\pm$ 5	0 $\pm$ 3		$f$ ( $\mu$ N)	66 $\pm$ 4	180 $\pm$ 10	0 $\pm$ 3
R360	$h$ (mm)	1.63	2.7	3.92	R5000	$h$ (mm)	1.63	2.68	5.31
	$2r_{tpc}$ (mm)	1.44	0.79	0.27		$2r_{tpc}$ (mm)	1.78	1.31	0.37
	$\theta$ (°)	39.00	75.00	95.00		$\theta$ (°)	78.00	93.00	109.00
	$f$ ( $\mu$ N)	86 $\pm$ 10	150 $\pm$ 10	0 $\pm$ 3		$f$ ( $\mu$ N)	26 $\pm$ 3	218 $\pm$ 10	0 $\pm$ 4

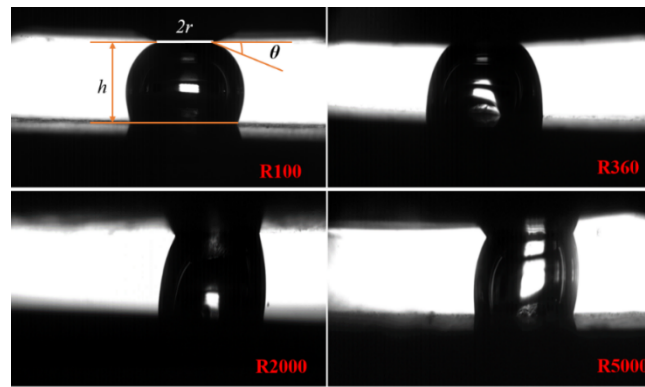


Fig. 10. The interaction state between air bubble and coal surface of different roughness at point C

As also presented in Table 2, the magnitude of interaction force ( $f$ ) correspondingly increased with the increase of surface roughness within 2-10 sec. The force magnitude between air bubble and coal surfaces of R100, R360, R2000, and R5000 were 150 $\pm$ 10  $\mu$ N, 86 $\pm$ 10  $\mu$ N, 66 $\pm$ 4  $\mu$ N, 26 $\pm$ 3  $\mu$ N, respectively. In other words, the greater deformation of air bubble during bubble-particle attachment resulted from the smaller adhesion diameters, and led to the larger magnitude of the upward force.

It has also been proved by many researchers that the contact line would be pinned when meeting the edges (Dettre and Johnson, 1964; David and Neumann, 2013) and the stronger pinning for the TPCL would be for the rougher surfaces (Chung et al., 2007; Sun et al., 2018). However, Albijanic et al. (2010) concluded that the time consumed of expansion of TPCL at surface with roughness below 50-80  $\mu$ m was shorter than that at surface with roughness below 30-60  $\mu$ m. They considered that the formation velocity of critical thickness of liquid film was promoted by larger asperities at rougher surface. And, the entrapped gas at the rougher surfaces also eased the rupture of liquid film. Hassas et al. (2018) also studied the influence of CO<sub>2</sub> on bubble attachment at fresh pyrite surfaces. They considered that CO<sub>2</sub> bubbles had a propensity to spread and their presence at the fresh pyrite surface subsequently facilitated the film rupture and the attachment of bubbles on pyrite surface. As a result, the flotation of pyrite was improved. Other studies (Guvén et al., 2015; Karakas and Hassas, 2016) also proved that flotation rate constant increased with the increase of surface roughness. Nona-bubbles entrapped in the rough surfaces would increase the hydrophobic force, which resulted in spontaneous spreading of TPCL. In this study, since the micro-bubbles that grew on the surfaces were wiped off when the surfaces were immersed in water, and the ridges and grooves on surfaces were filled up with water, so there formed a thin water film that prevented the formation and expansion of the TPCL (Schmidt and Berg, 1997).

### 3.4.3. Analysis of interactions in the process of air bubble moving downward

From the beginning of 10 sec, the elevating table was motored downwards, and the bubble immediately exerted a downward pulling force on the sample, changing the state of air bubble from static to receding.

As also shown in Fig. 8, the maximum detachment force (the maximum detachment force point was designated as point D) were  $53 \pm 5 \mu\text{N}$ ,  $150 \pm 10 \mu\text{N}$ ,  $180 \pm 10 \mu\text{N}$ , and  $218 \pm 10 \mu\text{N}$ , respectively, as roughness index decreased from 2.51 to  $0.12 \mu\text{m}$ . The maximum detachment force with the direction of downward decreased with the increase of surface roughness in the process of air bubble moving downward. Otherwise, the biggest detachment force was found between air bubble and the R5000 surface while the smallest detachment force occurred on the R100 surface. This is similar to the process of advancing contact angle measurement in which the pinning of the TPCL by ridges and grooves prohibited the receding of air bubble. Moreover, many researchers (Dettre and Johnson, 1964; David and Neumann, 2013; Moraila et al., 2019) thought that the "inverse" Cassie Model would present at the surface of a sufficient level of roughness as the degree of roughness increased, because some water was held in the ridges and grooves, hence the actual adhesion area between surface and air bubble was less than the apparent adhesion area. Moreover, another reason is that the adhesion diameter at point D decreased with the increasing of the degree of roughness, as shown in Fig. 11. It is also presented in Table 2 that the maximum adhesion diameter exerted between the air bubble and R5000 surface was about 1.31 mm, while the minimum adhesion diameter was only 0.68 mm between air bubble and R100 surface. The adhesion diameter between the four surfaces of different roughness reduced compared with that at point C. Evidently, this phenomenon should be further studied.

Figure 12 shows the interaction state between air bubble and coal surface of different roughness at point E, the pull-off distance between air bubble and coal surface was shown to steadily increase from 3.72 mm to 3.92 mm, 4.13 mm, to 5.31 mm with the decrease of the degree of roughness.

At last, the force returned to near zero after the bubble detached from the surface. It must be noted that there were micro-bubbles produced on these four surfaces except R100 as soon as the bubble detached from the coal surface (Fig.13).

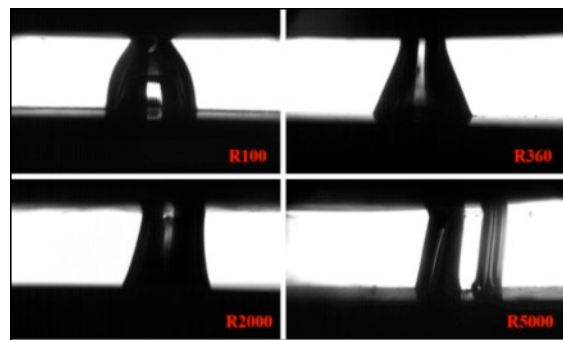


Fig. 11. Interactions state between air bubble and coal surface of different roughness at point D

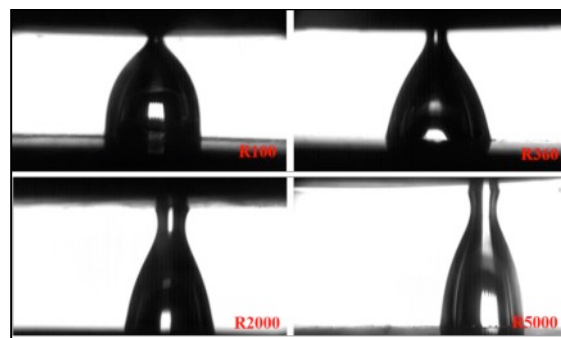


Fig. 12. Interactions state between air bubble and coal surface of different roughness at point E

#### 3.4.4. Calculation of interaction force between air bubble and coal surface of different roughness

The interaction force between the air bubble and solid surface consists of two categories: The ones with the direction of upward, including the force of buoyancy and counter capillary pressure; while the ones with the direction of downward included the force of gravity and counter surface tension. The resultant force acting on the surface was detected by the microbalance and was defined by Eq. 1 (Nguyen, 2004;

Wang et al., 2016):

$$\vec{F}_r = \vec{F}_f + \vec{F}_c + \vec{F}_g + \vec{F}_s \quad (1)$$

where  $\vec{F}_r$ ,  $\vec{F}_f$ ,  $\vec{F}_c$ ,  $\vec{F}_g$ , and  $\vec{F}_s$  are the resultant, buoyancy force, counter capillary pressure, gravity force, and counter surface tension, respectively. Since the influence of gravity and buoyancy force was eliminated by subtracting the background test values. As a result, the equation can be defined as Eq. 2:

$$\vec{F}_r = \vec{F}_c + \vec{F}_s \quad (2)$$

The vertical component of the counter surface tension is the liquid-gas interfacial tension acting along the perimeter of triple contact line. The relevant expressions for  $\vec{F}_s$  is:

$$\vec{F}_s = 2\pi r_{tpc} \gamma \sin\theta \quad (3)$$

The counter capillary pressure force ( $\vec{F}_c$ ) is caused by the curvature of the liquid bridge. The relevant expressions for  $\vec{F}_c$  is:

$$\vec{F}_c = -\pi r_{tpc}^2 \Delta P \quad (4)$$

The minus sign occurs in this equation because the force acted upwards on the sample. Where  $\Delta P$  is the Young-Laplace pressure. Thus, Eq. 2 can also be expressed in Eq. 5:

$$\vec{F}_r = 2\pi r_{tpc} \gamma \sin\theta - \pi r_{tpc}^2 \Delta P \quad (5)$$

The Young-Laplace pressure can be calculated as following:

- If the air bubble shows a convex profile:

$$\Delta P = \gamma \left( \frac{1}{D} + \frac{1}{R} \right) \quad (6)$$

- If the air bubble shows a concave profile:

$$\Delta P = \gamma \left( \frac{1}{D} - \frac{1}{R} \right) \quad (7)$$

It should be mentioned that it is an approximate method to calculate the capillary forces using two main curvature radii, but it is actually a valid simplification in the analysis (Fig. 14).

Table 3 presents the experimental and calculated force magnitude  $F_r$  at point  $D$  for coal surface of different roughness along with the parameters measured and used in the calculation. As shown in Table 3. The last column presents the difference between  $F_r$  values that measured directly and calculated. The

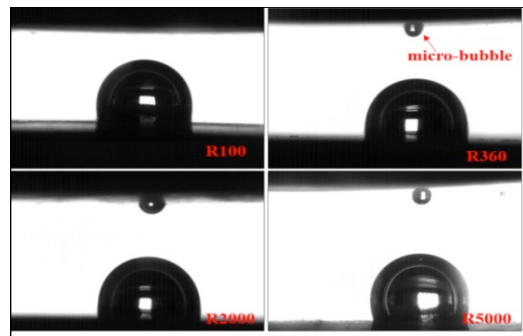


Fig. 13. Presence of micro-bubbles produced after pull-off of coal surface (R360, R2000, and R5000)

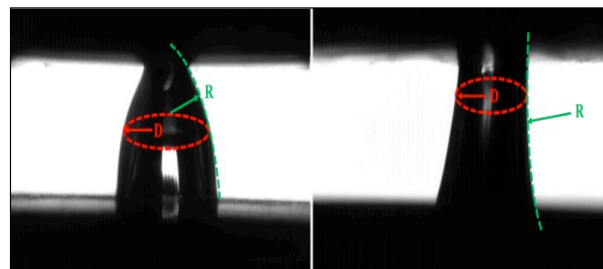


Fig. 14. Curvature radii  $D$  and  $R$  of two shapes of air bubbles

agreement was within about 32%. The differences between the calculated and experimental force values are likely ascribed to the limited accuracy of the microbalance in determination of forces caused by errors in contact angle, radius of air bubble, surface curvature, and adhesion diameter measurements that need to be carried out on captured images. In addition, adhesion diameters achieved only in the direction of perpendicular with grooves and the adjusting shape of TPCL to topographic feature resulting from surface roughness are also corresponding to the differences. The differences caused by roughness should be further studied. However, the calculated force magnitude also increased with the decrease of surface roughness.

Table 3. Calculated and experimental force  $F_r$  value at point  $D$  for coal surface of different roughness

Samples	$2r_{tpc}$ (mm)	$\theta$ (°)	$\gamma$ (mN/m)	$F_s$ ( $\mu$ N)	$D$ (mm)	$R$ (mm)	$\Delta P$ (kN/m)	$F_c$ ( $\mu$ N)	$F_{r,cal}$ ( $\mu$ N)	$F_{r,exp}$ ( $\mu$ N)	$F_{diff}$ ( $\mu$ N)
R100	0.68	63.00	72.40	137.81	0.46	1.97	194.14	-70.51	67.30	53.00	14.30
R360	0.79	75.00	72.40	173.56	0.55	4.54	147.58	-72.34	101.22	150.00	-48.78
R2000	1.12	91.00	72.40	254.71	0.69	5.21	91.03	-89.68	165.02	180.00	-14.98
R5000	1.31	93.00	72.40	297.55	0.72	7.18	90.47	-121.94	175.61	218.00	-42.39

### 3.4.5. Comparison and analysis of contact angle

The results of contact angle measured by bubble captive method and contact angles measured in the process of air bubble continuous interaction with coal surface of different roughness are summarized in Table 4. As shown in Table 4, the contact angle measured by Image J in the process of air bubble approaching was in correction with the receding contact angle. However, the contact angle at point  $C$  was bigger than the receding contact angle, which is probably due to the fact that the upward force drove the spreading of TPCL, which was derived from the deformation of air bubble. Meanwhile, the advancing contact angle was in corresponding with the contact angle at maximum adhesion point (point  $D$ ) and then pull-off (point  $E$ ) for surfaces of different roughness.

Table 4. The results of contact angle measured by captive-bubble method and contact angle measured in the process of air bubble continuous interaction with coal surface of different roughness

Samples	Receding contact angle (°)		Advancing contact angle (°)		
	$\theta_r$	$\theta_C$	$\theta_{ad}$	$\theta_D$	$\theta_E$
100	30	31	78	63	68
360	47	39	84	75	95
2000	57	64	89	91	108
5000	68	78	93	93	109

## 4. Conclusions

In this study, the continuous interaction between air bubble and coal surface of different roughness was measured by a highly sensitive microbalance, coupled with a high-speed video camera to capture the shape changes of air bubbles. The advancing and receding contact angles in the direction of perpendicular ( $\phi_{\perp}$ ) with grooves were measured by captive bubble method. Both the advancing and receding contact angles decreased with the increase of surface roughness. Moreover, in the continuous attachment and detachment process between air bubble and coal surface, the force between the air bubble and the coal surface showed good correlation to the degree of surface roughness. It increased consistently with surface roughness in the process of air bubble moving upward and remaining stationary, while it decreased with the degree of roughness in the process of air bubble moving downward. Therefore, it was also concluded that the surface roughness had a significant effect on the force between air bubble and coal surface. On the other hand, the attachment time between air bubble and coal surface increased with the increase of surface roughness. It may be related to the thin water film exerted in the ridges and grooves that prevented the formation and expansion of the TPCL. The

adhesion diameters at different points between air bubble and coal surface decreased with the increase of roughness. Meanwhile, it was also demonstrated that the actual adhesion area between air bubble and surface was less than the apparent adhesion area, resulting from the “inverse” Cassie Model, which occurred at a sufficient level of roughness. Furthermore, the interaction force was also calculated. The calculated resultant force also increased with the decrease of surface roughness, which was consistent with the force measured in the experimental system. The difference between the measured and calculated force might be due to the adjustment of the shape of TPCL to the topographic feature, which changed the actual length of TPCL. These results indicated that coal particles with lower surface roughness is more conducive to flotation and vice versa. Because water-filled pores and pillars on the surface have negative effects on bubble-particle interaction force.

### Acknowledgements

This work was supported by the Fundamental Research Funds for the Central Universities (2017CXNL04).

### References

- ADAMS, D.J., ADAMS, S., MELROSE, J., WEAVER, A.C., 2008. *Influence of particle surface roughness on the behaviour of Janus particles at interfaces*. *Colloids Surfaces A Physicochem. Eng. Asp.* 317, 360–365.
- ALBIJANIC, B., OZDEMIR, O., NGUYEN, A. V, BRADSHAW, D., 2010. *A review of induction and attachment times of wetting thin films between air bubbles and particles and its relevance in the separation of particles by flotation*. *Adv. Colloid Interface Sci.* 159, 1–21.
- BORMASHENKO, E., 2019. *Apparent contact angles for reactive wetting of smooth, rough, and heterogeneous surfaces calculated from the variational principles*. *J. Colloid Interface Sci.* 537, 597–603.
- CHANG, Z., CHEN, X., PENG, Y., 2017. *Understanding and improving the flotation of coals with different degrees of surface oxidation*. *Powder Technol.* 321, 190–196.
- CHAU, T.T., BRUCKARD, W.J., KOH, P.T.L., NGUYEN, A. V, 2009. *A review of factors that affect contact angle and implications for flotation practice*. *Adv. Colloid Interface Sci.* 150, 106–115.
- CHEN, S., TANG, L., TAO, X., CHEN, L., YANG, Z., LI, L., 2017. *Effect of oxidation processing on the surface properties and floatability of Meizhiyou long-flame coal*. *Fuel* 210, 177–186.
- CHEN, Y., XIA, W., XIE, G., 2018. *Contact angle and induction time of air bubble on flat coal surface of different roughness*. *Fuel* 222, 35–41.
- CHIPFUNHU, D., ZANIN, M., GRANO, S., 2011. *The dependency of the critical contact angle for flotation on particle size - Modelling the limits of fine particle flotation*. *Miner. Eng.* 24, 50–57.
- CHUNG, J.Y., YOUNGBLOOD, J.P., STAFFORD, C.M., 2007. *Anisotropic wetting on tunable micro-wrinkled surfaces*. *Soft Matter* 3, 1163.
- DAVID, R., NEUMANN, A.W., 2013. *Energy barriers between the Cassie and Wenzel states on random, superhydrophobic surfaces*. *Colloids Surfaces A Physicochem. Eng. Asp.* 425, 51–58.
- DETTRE, R.H., JOHNSON JR., R.E., 1964. *Contact Angle Hysteresis*. *Prog. Surf. Membr. Sci.* 6, 125–138.
- DRELICH, J., MILLER, J.D., Good, R.J., 1996. *The effect of drop (bubble) size on advancing and receding contact angles for heterogeneous and rough solid surfaces as observed with sessile-drop and captive-bubble techniques*. *J. Colloid Interface Sci.* 179, 37–50.
- DRELICH, J.W., 2018. *A simplified analysis of the effect of nano-asperities on particle-bubble interactions*. *Physicochem. Probl. Miner. Process.* 54, 10–18.
- DRELICH, J.W., MARMUR, A., 2017. *Meaningful contact angles in flotation systems: critical analysis and recommendations*. *Surf. Innov.* 6, 19–30.
- ERBIL, H.Y., 2014. *The debate on the dependence of apparent contact angles on drop contact area or three-phase contact line: A review*. *Surf. Sci. Rep.* 69, 325–365.
- FENG, D.X., NGUYEN, A.V., 2017. *Effect of contact angle and contact angle hysteresis on the floatability of spheres at the air-water interface*. *Adv. Colloid Interface Sci.* 248, 69–84.
- GOSIEWSKA, A., DRELICH, J., Laskowski, J.S., Pawlik, M., 2002. *Mineral matter distribution on coal surface and its effect on coal wettability*. *J. Colloid Interface Sci.* 247, 107–116.
- GUVEN, O., CELIK, M.S., DRELICH, J.W., 2015. *Flotation of methylated roughened glass particles and analysis of particle-bubble energy barrier*. *Miner. Eng.* 79, 125–132.

- HAN, O.H., KIM, M.K., KIM, B.G., SUBASINGHE, N., PARK, C.H., 2014. *Fine coal beneficiation by column flotation*. Fuel Process. Technol. 126, 49–59.
- HASSAS, B.V., JIN, J., DANG, L.X., WANG, X., MILLER, J.D., 2018. *Attachment, Coalescence, and Spreading of Carbon Dioxide Nanobubbles at Pyrite Surfaces*. Langmuir 34, 14317–14327.
- JOHNSON, D.J., MILES, N.J., HILAL, N., 2006. *Quantification of particle – bubble interactions using atomic force microscopy: A review*. Adv. Colloid Interface Sci. 127, 67–81.
- KARAKAS, F. and HASSAS, B.V., 2016. *Effect of surface roughness on interaction of particles in flotation*. Physicochem. Probl. Miner. Process. 52, 18–34.
- KARAKASHEV, S.I., STÖCKELHUBER, K.W., TSEKOV, R., 2011. *Journal of Colloid and Interface Science Wetting films on chemically patterned surfaces*. J. Colloid Interface Sci. 363, 663–667.
- KRASOWSKA, M., MALYSA, K., 2007. *Kinetics of bubble collision and attachment to hydrophobic solids: I. Effect of surface roughness*. Int. J. Miner. Process 81, 205–216.
- LIU, D., PENG, Y., 2014. *Reducing the entrainment of clay minerals in flotation using tap and saline water*. Powder Technol. 253, 216–222.
- LIU, J., HOLUSZKO, M., MASTALERZ, M., 2017. *Applications of micro-FTIR technique in studying hydrophobicity of coal*. Int. J. Coal Geol. 178, 74–83.
- MORAILA, C.L., RUIZ-CABELLO, F.J.M., CABRERIZO-VILCHEZ, M., RODRIGUEZ-VALVERDE, M.Á., 2019. *Wetting transitions on rough surfaces revealed with captive bubble experiments. The role of surface energy*. J. Colloid Interface Sci. 539, 448–456.
- NGUYEN, A.V., 2004. *Colloidal Science of flotation*. Taylor & Francis Group.
- NIKOLAEV, A., 2016. *International Journal of Mineral Processing Flotation kinetic model with respect to particle heterogeneity and roughness*. Int. J. Miner. Process. 155, 74–82.
- OSASERE ORUMWENSE, F., 1998. *Estimation of the wettability of coal from contact angles using coagulants and flocculants*. Fuel 77, 1107–1111.
- PIETRZAK, R., WACHOWSKA, H., 2006. *The influence of oxidation with HNO<sub>3</sub> on the surface composition of high-sulphur coals: XPS study* 87, 1021–1029.
- SAMUEL, B., ZHAO, H., LAW, K.Y., 2011. *Study of wetting and adhesion interactions between water and various polymer and superhydrophobic surfaces*. J. Phys. Chem. C 115, 14852–14861.
- SCHMIDT, D. C., BERG, J.C., 1997. *Selective removal of toner particles from repulped slurries by flotation: they react differently from spheres*. Soc. Policy Soc. (98)2, 21–24.
- SUN, Y., DRELICH, J.W., XIE, G., JIANG, Y., CHOI, C.H., LIU, Q., 2018. *The most stable state of a droplet on anisotropic patterns: Support for a missing link*. Surf. Innov. 6, 133–140.
- SUN, Y., JIANG, Y., CHOI, C.-H., XIE, G., LIU, Q., DRELICH, J.W., 2017. *Direct Measurements of Adhesion Forces for Water Droplets in Contact with Smooth and Patterned Polymers*. Surf. Innov. 6, 1–52.
- ULUSOY, U., YEKELER, M., HIÇYILMAZ, C., 2003. *Determination of the shape, morphological and wettability properties of quartz and their correlations*. Miner. Eng. 16, 951–964.
- WEANG, G., EVANS, G.M., JAMESON, G.J., 2017. *Bubble-particle detachment in a turbulent vortex II – Computational methods*. Miner. Eng. 102, 58–67.
- WANG, G., FENG, D., NGUYEN, A., EVANS, G.M., 2016. *The dynamic contact angle of a bubble with an immersed-in-water particle and its implications for bubble-particle detachment*. Int. J. Miner. Process. 151, 22–32.
- WANG, S., GUO, J., TANG, L., HE, H., TAO, X., 2018. *Effect of surface roughness of Chinese sub-bituminous coal on the kinetics of three-phase contact formation*. Fuel 216, 531–537.
- XIA, W., 2017a. *Role of particle shape in the floatability of mineral particle: An overview of recent advances*. Powder Technol. 317, 104–116.
- XIA, W., 2017b. *Role of surface roughness in the attachment time between air bubble and flat ultra-low-ash coal surface*. Int. J. Miner. Process. 168, 19–24.
- XIA, W., XIE, G., LIANG, C., YANG, J., 2014. *Flotation behavior of different size fractions of fresh and oxidized coals*. Powder Technol. 267, 80–85.
- XING, Y., GUI, X., PAN, L., PINCHASIK, B., CAO, Y., LIU, J., 2017. *Recent experimental advances for understanding bubble-particle attachment in flotation*. Adv. Colloid Interface Sci. 246, 105–132.
- ZHOU, Y., ALBIJANIC, B., TADESSE, B., WANG, Y., YANG, J., LI, G., ZHU, X., 2019. *Surface hydrophobicity of sub-bituminous and meta-bituminous coal and their flotation kinetics*. Fuel 242, 416–424.